Carbon, Volume 167, October 2020, pp. 114-121
DOI:10.1016/j.carbon.2020.04.086

Distribution of shallow NV centers in diamond revealed by photoluminescence spectroscopy and nanomachining

Majid Fazeli Jadidi[1], H. Özgür Özer[2], Saurav Goel[3,4], Jason I. Kilpatrick[1], Niall McEvoy[5], David McCloskey[5,6], John F. Donegan[5,6], Graham L. W. Cross[*,1,5,6]

[1]Adama Innovations Ltd., CRANN, Trinity College Dublin, Dublin 2, Ireland

[2] Department of Physics Engineering, Istanbul Technical University, 34469, Maslak, Sarıyer, Istanbul, Turkey

[3] School of Engineering, London South Bank University, 103 Borough Road, London SE1 0AA, UK

[4] School of Aerospace, Transport and Manufacturing, Cranfield University, Cranfield, MK43 0AL, UK

[5] Advanced Materials and Bioengineering Research (AMBER) Centre, CRANN, Trinity College Dublin, Dublin 2, Ireland

[6] School of Physics, Trinity College Dublin, Dublin 2, Ireland

Abstract

We performed nanomachining combined with photoluminescence spectroscopy to understand the depth distribution of nitrogen-vacancy (NV) centers formed by low energy nitrogen ion irradiation of the diamond surface. NV^- and NV^0 fluorescence signals collected from the surface progressively machined by a diamond tip in an atomic force microscope (AFM) initially rise to a maximum at 5 nm depth before returning to background levels at 10 nm. This maximum corresponds to the defect depth distribution predicted by a SRIM simulation using a 2.5 keV

*Corresponding author. Tel: +353 (0)1 896 3024. E-mail: graham.cross@tcd.ie

implantation energy per nitrogen atom. Full extinguishing of implantation produced NV^- and NV^0 zero phonon line peaks occurred beyond 10 nm machining depth, coinciding with the end of easy surface material removal and onset of significant tip wear. The wear ratio of for NV active, ion irradiated diamond compared to the single-crystal diamond tip was surprisingly found to be 22:1. The reported results constitute the first integrated study of in-situ machining and wear characterization via optical properties of the diamond surface containing shallow formed NV centers. We discuss possible metrology applications for diamond tools used in precision manufacturing.

Keywords: NV center, N_2 irradiation, AFM nanomachining, diamond cantilever, photoluminescence spectroscopy

1. Introduction

Quantum sensing with diamond defects provides new ways to achieve in-process nanoscale property mapping with single atom sensitivity [1-5]. The nitrogen-vacancy (NV) center is a photo-stable point defect in diamond and is one of the most promising candidates for quantum sensing [6, 7] as well as solid-state qubits (quantum bits) [8-10]. This is due to robust quantum coherence with strong optical coupling where, for example, the electron spin in a single NV center has been shown to be optically readable at room temperature [11-13].

The NV center in diamond is an active colour center formed by placement of a nitrogen atom next to a vacancy in the diamond lattice [1]. It has two main charge states NV^0 and NV^- with zero phonon lines (ZPL) at 575 nm and 637 nm respectively. NVs are found naturally at low concentration in the diamond lattice. This concentration can be increased near a surface by

irradiating with electrons [14], neutrons [15], high energy ions [16, 17], or femtosecond laser pulses [18] and has even allowed high resolution patterning via direct beams [16]. An annealing step is usually used to diffuse the vacancies which are captured next to the nitrogen atoms to form the NV centers. Precise position and density control of the NV centers in the surface of diamond plays a key role for sensing applications. Some, such as high-resolution spin sensing with a scanned probe, requires very low concentrations (down to a single NV center at the end of a probe). In others, however, the local density must be maximised to improve signal-to-noise.

The exploitation of the NV center sensing to the diamond tooling industry has many salient benefits. Diamond cutting tools form the backbone of many precision manufacturing processes including single point diamond turning [19, 20], tip based imaging and nanomachining [21, 22]. Despite many atomistic modeling studies of these processes[4, 5], few high resolution metrologies exist that can characterize or monitor the nanoscopic diamond contact processes needed to verify theory.

In this work, we exposed a single crystal diamond surface to low energy N_2^+ ions in order to create excess NV centers to a ~10 nm depth below the surface. We then performed controlled nanomachining of a diamond using an atomic force microscope (AFM) with a sharpened single crystal diamond tip. Changes in the photoluminescence (PL) spectrum at the NV^0 and NV^- ZPL peaks we recorded as a function of machining depth using confocal scanning Raman microscopy. This provided a fresh and improved insight of the material removal processes via an in-process metrology technique. An unexpected localization of the NV fluorescence signal was observed, revealing a depth sensitivity to NV defect formation with nanometer scale resolution. Unlike highly specialized high resolution depth sensing techniques for NVs [23, 24], this approach allows relatively standard equipment to be employed to determine the local NV distribution. Thus, it

appears possible to use the NV fluorescence signal as a sensitive measure to fully characterize the nanoscale wear of diamond tools provided the NV density is low enough not to interfere with the mechanical integrity (weakening of the structure) required for manufacturing processes of hard, brittle materials.

2. Experimental method

A nitrogen doped single crystal CVD grown diamond (3x3 mm size, 0.5 mm thick, type Ib (100) oriented, polished diamond sample with nitrogen content >200 ppm, with <2 nm roughness measured) was used to study the creation of NV centers by ion irradiation. This process was accomplished in an ultra-high vacuum (UHV) chamber with base pressure of 10^{-9} mbar using a cold cathode irradiation source (Omicron ISE 5 ion source). The sample was irradiated with N_2^+ ions with a dose of $4x10^{15}$ ions/cm^2 with beam energy 5 keV. For purposes of performing the single atom scattering simulation described below, we assume that this energy is split equally between the two N atoms (ie. 2.5 keV each) [17]. The sample was annealed at 800°C for an hour immediately after irradiating to mobilize vacancies and form NV centers. The single crystal diamond with NV centers was then machined in order to investigate independently the depth profile of NV centers and to assess feasibility of use of NV centers as in-process sensing during a tribocontact. The machining of the diamond surface was achieved with Bruker multimode 8-HR AFM using stiff diamond cantilevers (produced by Adama Innovations Ltd. NMU-BC boron doped cantilever with spring constant of ~4500 N/m). All samples during pre- and post-machining were characterized using a PL Microscopy/Spectroscopy (WITec alpha 300 R confocal Raman system). The range of ions and created vacancy density and distribution in diamond was simulated with SRIM , a widely used software package for calculating the path and range of energetic ions in matter [25, 26]. The depth resolution of the scanned confocal microscope was determined by

the objective lens numerical aperture (NA) and exciting laser wavelength λ to be λ/NA^2 = $532nm/0.95^2 \approx 590\ nm$.

3. Results and Discussion

3.1 Formation of shallow NV centers

Plots of ion distribution, ion/recoil collision and vacancy distribution simulated using SRIM software are shown in Figure 1 for 100,000 nitrogen ions each with 2.5 keV kinetic energy impinging on a single point of the surface. The average number of vacancies created per ion were estimated to be 16. The SRIM simulation shows the maximum depth of vacancies to be up to 10 nm and that the maximum vacancy density occurred at a depth of 3 nm below the bombarded surface. Ion distribution graph shows the maximum density of implanted N ions is at a depth of 5 nm below surface.

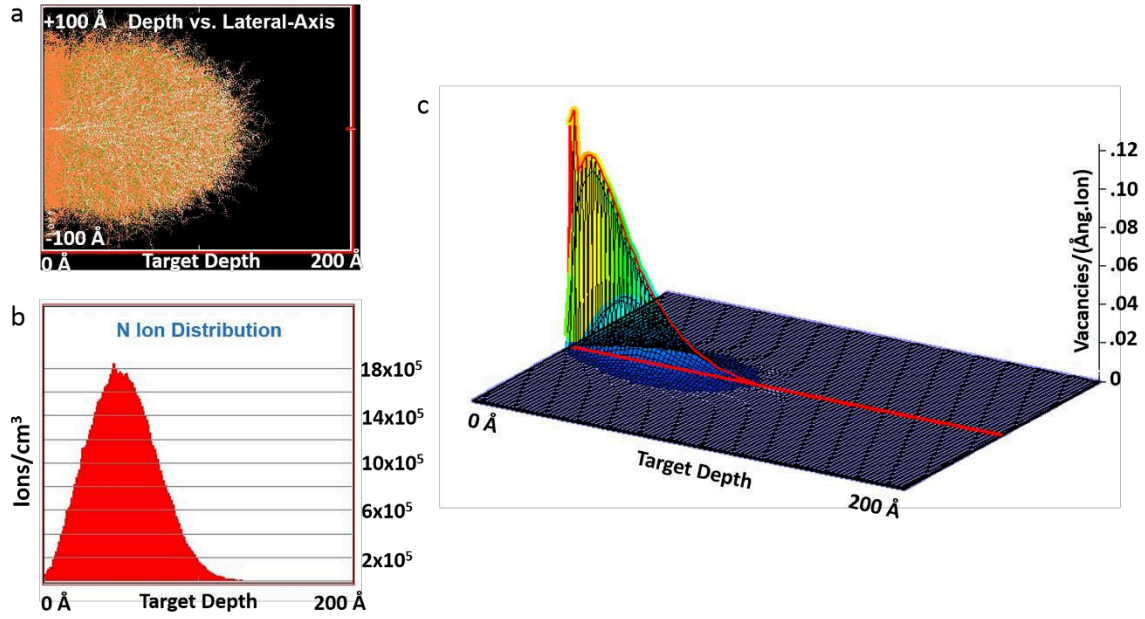

Figure 1: SRIM simulation results of 2.5 keV N ion irradiation on diamond sample. a) Ion range in matter b) N ion distribution and c) vacancy distribution.

Fig. 2 shows the results of N_2^+ ion irradiation in the presence of a molybdenum foil shadow mask that was placed to the right side of the single crystal diamond sample. The masked region, demarked by the dashed blue line in Figs. 2a-d, appears in the optical microscope image of Fig. 2a as a darker area. Scanning PL microscopy was performed in the area is demarked by the red box outline in the optical image, and images corresponding to the diamond, NV^0 and NV^- peaks of spatially representative spectra in Fig. 2e were extracted and are shown in Figs. 2b, c, and d respectively. The image, filtered to the first order peak at 573 nm of the PL spectra for diamond, is markedly darkened in the irradiated (ie. unmasked) vs. non-irradiated region. An opposite contrast appears for images filtered to NV fluorescence peaks which appear brighter on the irradiated side. In addition, a third region of intermediately bright diamond and maximally bright NV contrast occurs along a narrow (~4 μm) band just inside the mask edge.

The schematic in Fig. 2f provides our interpretation of the above observations of light interacting with the modified diamond sample. A ~10 nm top surface nitrogen implantation layer on the left-hand irradiated side is shown to be in a brown shade. We infer that the optical and geometric properties of this layer increase the interface reflectivity of the sample, leading to the brightening in the white-light optical illumination (black arrows in figure 2f). The focused Raman excitation laser spot (shown in green) is affected by this layer in several ways. NV fluorescence occurs in it, accounting for the brighter NV peak contrast in the irradiated region (orange arrows). At the same time, evolution of diamond bond hybridisation from sp^3 to sp^2 is known to promote absorption of Raman excitation light [27], leading to a rapid extinguishing of the sp^3 peak signal that is otherwise emitted from the entire focusing volume over 0.5 μm deep (red arrows). A decrease in density of sp^3 diamond structure in favour of other C structures may result in an attenuation of either the excitation signal or the collected signal. The small peaks at about 586 nm (1756 cm^{-1}) and 601 nm

(2172 cm^{-1}) have been attributed to sp^2 carbon structures or defective diamond in CVD diamond films [28] and stretching of C-N triple bond [29], respectively, beside other peaks such as those from possible amorphous carbon in Raman spectra. These peaks disappear after machining the surface to a depth of about 15 nm (presented below.)

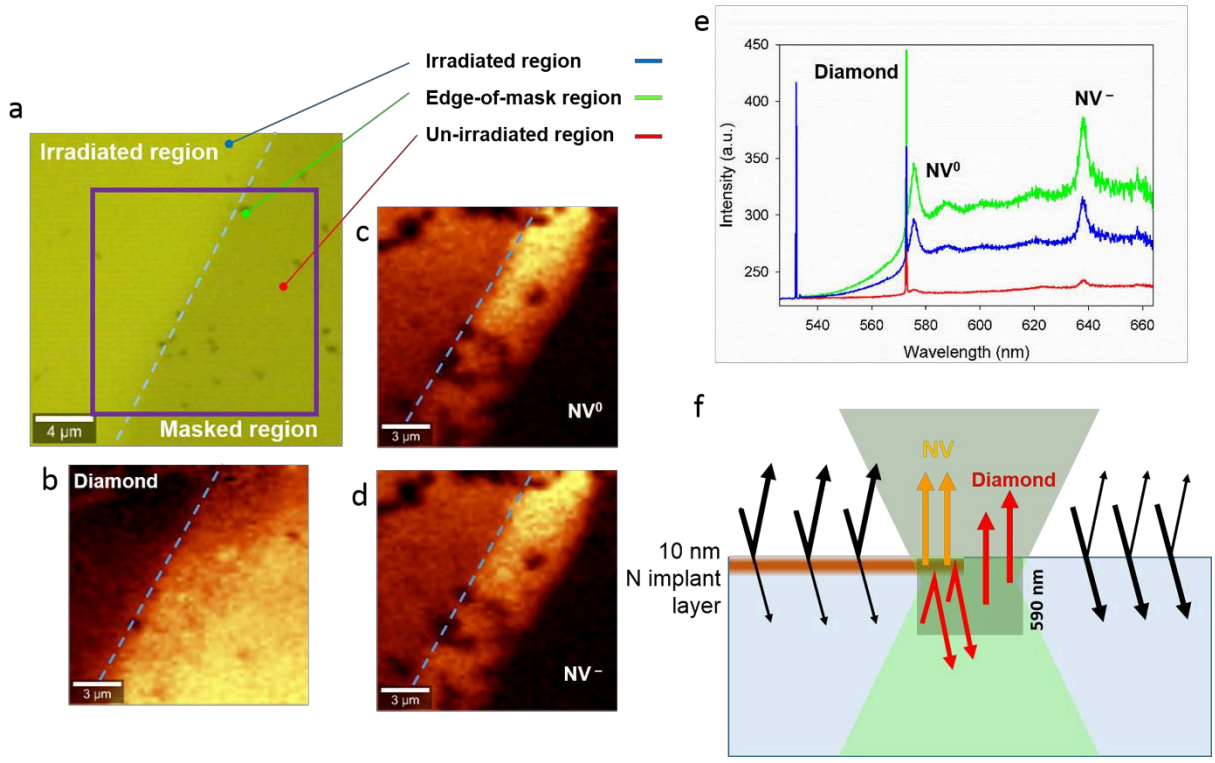

Figure 2: Scanning PL intensity analysis of nitrogen ion dosing of a partially masked diamond surface. a) Optical microscope image of diamond surface indicating PL scan area within the box. The lighter region to the left was irradiated, the region to the right was masked. The border of the mask is indicated by blue dashed lines in the images. (b-d) Scanning PL spectra images filtered to the b) peak at573 nm (diamond) c) NV^0 ZPL peak (575 nm) and d) NV^- ZPL peak (637 nm). Both NV^0 and NV^- fluorescence signals are significantly enhanced at the irradiated region. e) Average PL spectra at three distinct regions of dosing: un-irradiated (red), irradiated (blue) and border of

irradiated and un-irradiated (green). f) A schematic explaining the white-light optical (black arrows) and PL peak (orange and red) image contrast. See text for full explanation.

SRIM calculations show a lateral spread of N ions of only 20 nm within the diamond, thus the 4 μm contrast band inside the mask edge must be due to multiple scattering within the mask delivering a reduced ion dose to the diamond surface immediately below it. This multiple scattering can have lateral travel far exceeding expected vacancy diffusion: Contact mask edge spreading of over 10 μm was observed for MeV helium ions implanted into diamond, a distance far exceeding expected vacancy diffusion of a few 100 nm under annealing conditions similar to our own [31], and we have observed similar effects with low He ion implant energies [16, 32]. The enhanced brightness of the NV signals in this reduced flux region suggest that our 10^{15} ions/cm^2 irradiation was beyond an optimal NV formation dose, likely creating damage in the diamond lattice that reduced the population of NV defects. This is consistent with the findings of Pezzagna et al. [17] for 5 keV N ion bombardment where a dose of 1.2 x 10^{14} ions/cm^2 gave optimal NV fluorescence intensity. The image of Fig. 2b filtered to the 573 nm diamond peak also suggests a progressive sp^3 degradation gradient from the non-irradiated to fully irradiated region. We attribute the small, dark regions in the NV fluorescence peak images of Fig. 2c, d to inclusions and defects present near the CVD grown diamond surface. These are faint in the diamond peak image Fig. 2b and wholly absent in the white light image Fig. 2a as might be expected from features localized in depth.

3.2 Diamond Machining

The irradiated region was machined using the single crystal diamond AFM probe (fabricated by Adama Innovations Ltd. NMU-BC). The machining was carried out by raster scanning the surface in contact mode at constant scanning speed at different loads. Planar milling of squared regions visible in figure 3 (variable depths), was achieved by repeated scanning. Set loads of approximately 112.5, 157.5, 180 and 225 μN were used to achieve vertical machined depths of 3.5, 5, 7 and 8 nm respectively (as measured after the surface has sprung back).

In Fig. 3, the results of shallow machining are shown by AFM (figure 3a), optical microscope (figure 3b) and PL intensity images related to diamond (c), NV^0 (d) and NV^- (e) of squares. PL intensity images were extracted by filtering the measured scan results to the first order peak at 573 nm related to diamond with 1 nm bandwidth, NV^0 and NV^- ZPL peaks with 3 nm bandwidth and subtracting background. These consist of a 5x5 μm region machined to 2 nm depth, with a second, inner 3x3 μm region machined to 4 or 5 nm depths as determined directly from the AFM line scans. The white light optical image shows progressive darkening with depth, while all PL intensity images show an increase in brightness with depth. Deeper machining showed similar trends in all images except for the two NV signals, which instead darkened over depths of 3.5 nm, 5 nm, 7 nm and 8 nm, respectively: The white light darkened while the peak intensity related to diamond in PL spectra continued to brighten at these higher depths. The effect of machining in non-irradiated regions was also investigated with no observable effect on either white light or Raman optical signals save for a very slight increase in the diamond intensity in machined regions (see Fig.S1 in supplemental material). We attribute this to a change in surface roughness and/or contamination removal at the depths of 1 to 2 nm that could be achieved in a hard surface of diamond.

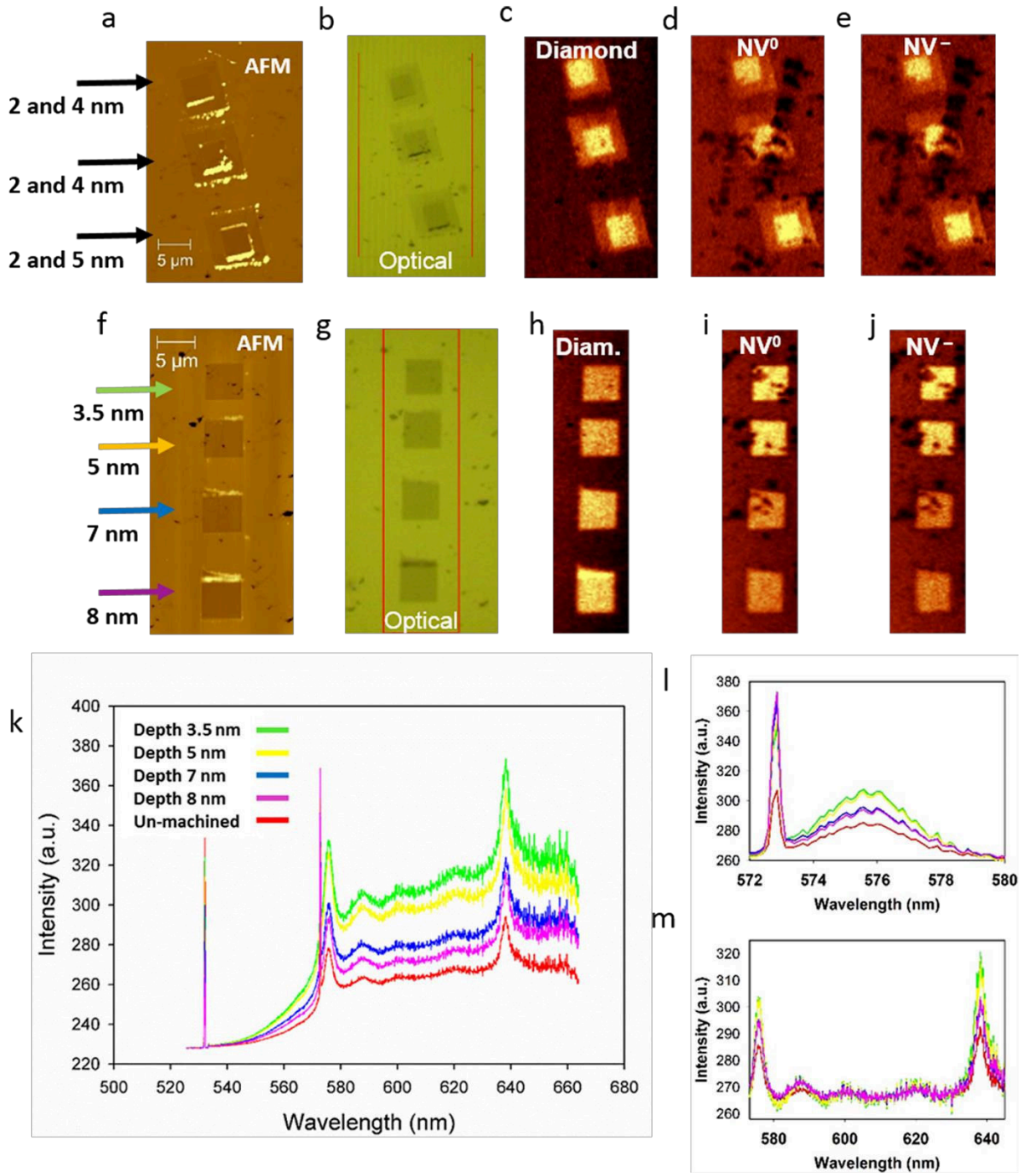

Figure 3: Machining in two different ranges of depth (panels a-e) vs (panels f to m). a) AFM image of 5x5 μm regions machined to 2 nm depth, with a second, inner 3x3 μm region machined to 4 or 5 nm depths (2/4, 2/4, and 2/5 nm outer/inner respectively from top to bottom) b) Optical

microscope image of diamond surface and with PL scan area indicated in red. Images of PL spectra filtered to the c) peak at 573 nm (diamond) d) NV^0 ZPL peak (575 nm) e) NV^- ZPL peak (637 nm). f) AFM image of 5x5 μm machined areas to deeper depths (3.5, 5, 7 and 8 nm respectively from top to bottom). g) Optical microscope image of diamond surface with PL scan area indicated in red. Images of PL spectra filtered to the h) peak at 573 nm (diamond) i) NV^0 ZPL peak (575 nm) j) NV^- ZPL peak (637 nm). k) Average PL spectra of unmachined and machined areas with different depths (unmachined:red, machined areas with the depth of 3.5nm: green, 5nm: yellow, 7nm: blue and 8nm: purple). l) and m) zoomed regions of graph shown in (k) after subtracting the background.

Collating all machining results of Fig. 3 together, we present the two NV ZPL peak intensities in Fig. 4(a) and the peak intensity related to diamond in PL spectra in Fig. 4(b), both as a function of machining depth and average PL signals. For purposes of this comparison, the average PL signal was normalised to the maximum value measured for each signal. The predictions of the SRIM simulation for the depth distribution of formed vacancies and stopping position of N ions is also shown in the lower panel, peaking at 3 and 5 nm respectively. The distribution of intensity with depth of the measured NV PL signals peaks at about 4 nm, interpolating the two SRIM calculations. Within the experimental error, the NV^0 and NV^- charge states show identical intensity depth distributions.

The observed trend of the diamond and NV relative intensities with nanomachining are consistent with Fig. 3f, where the effect of formation layer is to strongly localise the PL signal. The observation of a strong intensity peak with depth of the NV PL images in the first 10 nm of machining suggests a depth localisation of PL sensitivity to less than a nanometer. In the absence

of such localisation, both NV^0 and NV^- intensities are expected to simply decrease as the intense surface contribution is removed from the total background signal found in a diffraction limited volume which is normally expected to be probed by the PL imaging system. The diamond PL signal supports this interpretation: it monotonically increases with machining depth to return to the (absolute intensity) level of the unirradiated surface beyond the predicted 10 nm implantation limit. All NV PL intensity images in Fig. 3 contain small blackened regions which are absent in the diamond signal but are fully correlated between NV^0 and NV^-. We surmise that these are due to pre-existing defective crystal regions on or near the sample surface: In some instances such as the lower excavation in Fig. 3(j) they appear removed by machining, while in others they persist as in the excavation immediately above. We note that for the purposes of determining average intensities in Fig. 4(b), these black regions have been excluded. The absence of any black spots in the diamond Raman shift images is consistent with its signal being collected from light emitted from the entire confocal spot size into the sample, and not localized to the surface as in the fluorescence signals.

The relative charge stability of the NV^- and NV^0 defects are known to be sensitive to irradiation [34], doping with nitrogen [35] or phosphorus [36], and surface termination [23, 26]. Triboelectric current generation [37, 38] is well known in sliding contacts, with observation of an attractive force due to positive tribocharging for a diamond sliding on amorphous carbon surfaces [39, 40]. We observed no significant difference between evolving NV^- and NV^0 PL signal strength with machining depth, indicating charge stability of the defects to any triboelectric current generated.

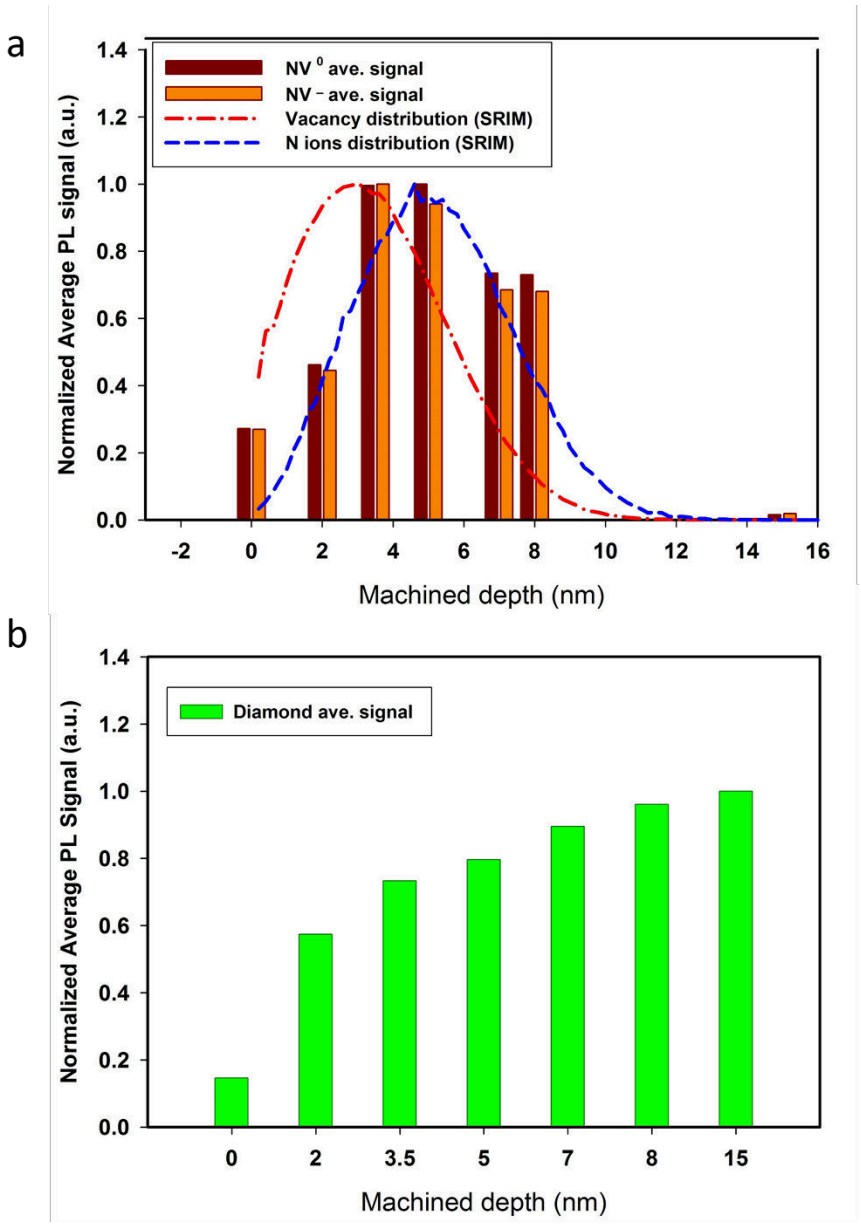

Figure 4: a) NV^- and NV^0 fluorescence peak distribution with depth compared to SRIM simulation calculations of vacancy and nitrogen ion implantation distribution. b) Average diamond PL signal collected over same depth range as (a).

In Fig. 5 we present the results of extended machining: 1200 scans of 5x5 μm of the irradiated surface lead to a total of 15 nm of material removal. The AFM topography and line profile (Fig. 5a) show side-to-side pileup of material at the edges of the fast scan direction. The largely flat

bottom of the machined crater has several deep nanoscale pits that we attribute to pre-existing inclusions left by the CVD forming process. The white-light optical, peak at 573 nm related to diamond and NV ZPL peaks in PL spectra (Fig. 5b, c, d, and e respectively) follow the same trends as the shallower excavations in Fig. 3. The NV^0 and NV^- signals in the machined region are highly attenuated save at a ridge along the lower left edge. This persistence may be due to ion travel into the inclusions pits located along this region.

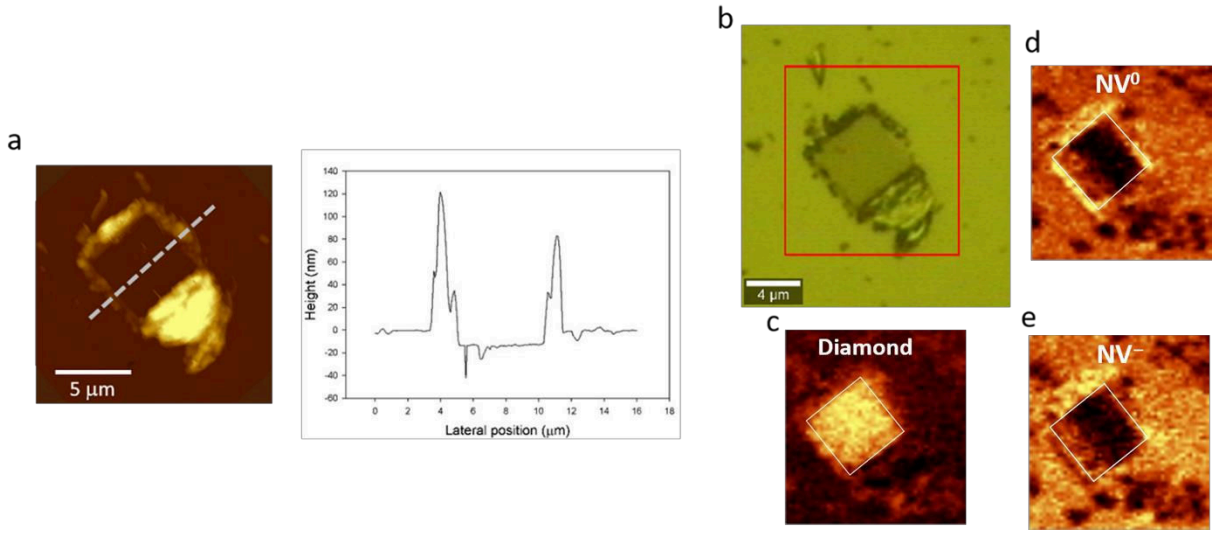

Figure 5: a) AFM image of a machined area after 1200 scans and the averaged line profile (grey dotted line in AFM image) showing inclusion defect pits on the left edge in an otherwise flat 15 nm excavation. b) Corresponding optical microscope image of machined diamond surface indicating 5×5 μm^2 PL scan area (red border). PL intensity scan images filtered to the d) peak at 573 nm (diamond) e) NV^0 ZPL peak (575 nm) f) NV^- ZPL peak (637 nm).

In Fig. 6 we plot the mean machining depth again number of image scans and total tip distance travelled corresponding to Fig. 5, along with before and after SEM images of the tip apex. The tip was initially scanned at low loads to allow imaging of the surface for 20 scans, followed by an increase to 1.35 mN for the subsequent 1180 scans. An initial rapid machining of 10 nm material

within 20 scans followed much more gradual removal. We surmise that two effects contributed to this: The full removal of surface material damaged by irradiation exposes harder, lower defect diamond below, and progressive dulling of the tip during machining. The effect of the latter can be seen in Fig. 6c.

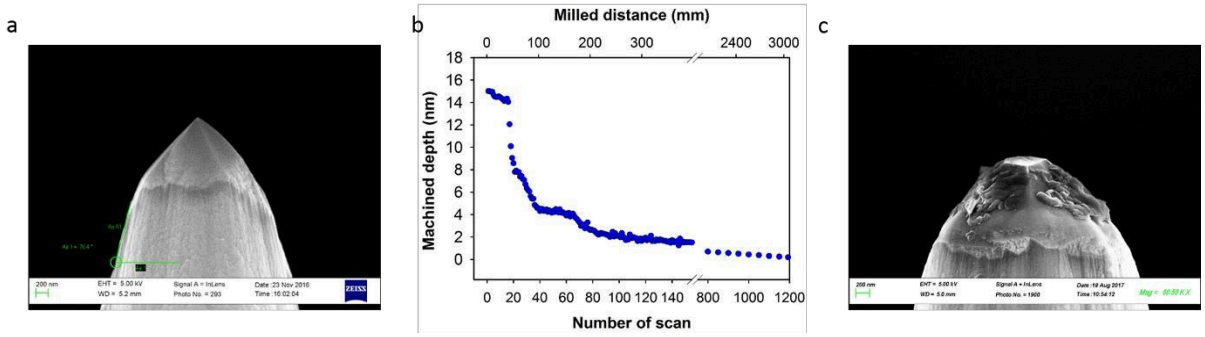

Figure 6: a) SEM images of single crystal diamond tip a) before and c) after machining the 5×5 μm^2 area of Fig. 5 to ~15 nm depth. Material removal depth with scan number and tip milling distance is shown in (b). After 20 initial low load scans, the tip load was increased to 1.35 mN leading to rapid removal of ~30 nm material with 20 more scan. Subsequent scanning (up to 1200 scans, not shown) resulted in only marginal further material removal.

From Fig. 6(c), the volume of material removed from the boron doped diamond tip after machining was estimated to be 0.014±0.002 μm^3, while the removed substrate volume was 0.31±0.03 μm^3 giving a substrate vs. tip wear ratio of ~22:1 over the large number of scans. While it is known that boron doping can improve the wear properties of diamond tools for plastics [42], the resilience of the tip is remarkable given the nominal hardness of the substrate material. The compression strength of (100) diamond micropillars was found to decrease about 25% under 30 keV helium radiation of fluence similar to our own [41], and we suspect the hardness of our substrate material will undergo significant weakening similar to this. Due to the nanoscopic dimension of the contact, we suspect both substrate and tip size effects to interfere with defect operation and increase

strength as noted previously for diamond [43]. The relative degree of this in each case is not known, however.

With regards to using surface NV concentrations as quantum sensing elements to measure wear in precision diamond tools *ex situ*, or eventually as an *in situ* local monitor of electromagnetic fields, temperature or pressure [44], a careful balance between tool mechanical integrity and NV concentration for sensing will have to be considered. The production of NVs by implantation may lead to excess damage [45], and other recently developed techniques such as delta-doping may hold more promise [46]. We believe the approach may have particular advantage for precision machining of polymers and soft matter where control of temperature and pressure are of extreme importance [47].

4. Conclusions

A surface of single crystal diamond was irradiated with N_2^+ ions in the (100) orientation and was studied by in-situ micro-PL spectroscopy after atomic scale nanomachining. The evolution of fluorescence signals under machining of diamond revealed a distribution of NV centers with depth initially increasing to 3-4 nm and then decreasing, while the peak related to diamond in PL spectra showed a monotonic increase in intensity with depth. The PL intensity peaks of both NV charge states were consistent with SRIM simulations of vacancy and nitrogen implantation expected distribution at the 2.5 keV energy used in experiment, with no sign of a differential influence arising from possible triboelectric effects. A peak machining depth of ~15 nm was observed after 1200 scans. Comparison of the excavated volume of the N_2^+ ion irradiated diamond surface with that from the single crystal diamond tip revealed a surprising wear ratio of 22:1. The diamond substrate appears to weaken significantly with the introduction of NV centers via ion bombardment at our dose of $4x10^{15}$ ions/cm^2 at 5 keV energy per N_2^+ ion. Thus using implantation to enable in-

situ quantum metrology for nanomachining may be more appropriate for soft matter work pieces than hard, brittle materials. Reducing the dose while maintaining fluorescent signal strength will be an important consideration for the use of the NV centers as a stable, *in situ* sensing element for diamond tools in those cases where mechanical strength is essential. Overall, we suggest that quantum sensing can be applied to understand tribological processes in important ultra-precision machining and imaging applications where the use of diamond tips is ubiquitous.

Acknowledgments

HOO acknowledges support of TÜBİTAK (2219/1059B191600977) and Istanbul Technical Univesity (BAP 39973). SG acknowledges support from the UKRI (Grants No.: EP/K503241/1, EP/L016567/1, EP/S013652/1, EP/T001100/1, EP/S036180/1 and EP/T024607/1), H2020 (Cost Actions (CA18125, CA18224 and CA16235) and EURAMET EMPIR A185 (2018)), Royal Academy of Engineering Grant No. IAPP18-19\295 (Indo-UK partnership) and Grant No. TSP1332 (South Africa- UK partnership), and Newton Fellowship award from the Royal Society (NIF\R1\191571).

References

[1] T. Schröder, S. Mouradian, J. Zheng, M.E. Trusheim, M. Walsh, E.H. Chen, L. Li, I. Bayn, D. Englund, Review Article: Quantum Nanophotonics in Diamond, arXiv [quant-ph] (2016).

[2] R. Schirhagl, K. Chang, M. Loretz, C.L. Degen, Nitrogen-vacancy centers in diamond: nanoscale sensors for physics and biology, Annu. Rev. Phys. Chem. 65 (2014) 83-105.

[3] P. Maletinsky, S. Hong, M.S. Grinolds, B. Hausmann, M.D. Lukin, R.L. Walsworth, M. Loncar, A. Yacoby, A robust scanning diamond sensor for nanoscale imaging with single nitrogen-vacancy centres, Nat. Nanotechnol. 7(5) (2012) 320-324.

[4] G. Moras, A. Klemenz, T. Reichenbach, A. Gola, H. Uetsuka, M. Moseler, L.J.P.R.M. Pastewka, Shear melting of silicon and diamond and the disappearance of the polyamorphic transition under shear, Phys. Rev. Materials, 2(8) (2018) 083601.

[5] S. Goel, G. Cross, A. Stukowski, E. Gamsjäger, B. Beake, A.J.C.M.S. Agrawal, Designing nanoindentation simulation studies by appropriate indenter choices: Case study on single crystal tungsten, Computational Materials Science, 152 (2018) 196-210.

[6] M.W. Doherty, N.B. Manson, P. Delaney, F. Jelezko, J. Wrachtrup, L.C.J.P.R. Hollenberg, The nitrogen-vacancy colour centre in diamond, Physics Reports, 528(1) (2013) 1-45.

[7] A. Gruber, A. Dräbenstedt, C. Tietz, L. Fleury, J. Wrachtrup, C.J.S. Von Borczyskowski, Scanning confocal optical microscopy and magnetic resonance on single defect centers, Science, 276(5321) (1997) 2012-2014.

[8] M.G. Dutt, L. Childress, L. Jiang, E. Togan, J. Maze, F. Jelezko, A. Zibrov, P. Hemmer, M.J.S. Lukin, Quantum register based on individual electronic and nuclear spin qubits in diamond, Science, 316(5829) (2007) 1312-1316.

[9] R. Hanson, V. Dobrovitski, A. Feiguin, O. Gywat, D.J.S. Awschalom, Coherent dynamics of a single spin interacting with an adjustable spin bath, Science, 320(5874) (2008) 352-355.

[10] P. Neumann, N. Mizuochi, F. Rempp, P. Hemmer, H. Watanabe, S. Yamasaki, V. Jacques, T. Gaebel, F. Jelezko, J.J.s. Wrachtrup, Multipartite entanglement among single spins in diamond, Science, 320(5881) (2008) 1326-1329.

[11] F. Jelezko, J.J.p.s.s. Wrachtrup, Single defect centres in diamond: A review, phys. stat. sol. (a), 203(13) (2006) 3207-3225.

[12] T. Kennedy, J. Colton, J. Butler, R. Linares, P.J.A.P.L. Doering, Long coherence times at 300 K for nitrogen-vacancy center spins in diamond grown by chemical vapor deposition, Appl. Phys. Lett., 83(20) (2003) 4190-4192.

[13] G. Balasubramanian, P. Neumann, D. Twitchen, M. Markham, R. Kolesov, N. Mizuochi, J. Isoya, J. Achard, J. Beck, J.J.N.m. Tissler, Ultralong spin coherence time in isotopically engineered diamond, Nature Materials, 8(5) (2009) 383.

[14] C.A. McLellan, B.A. Myers, S. Kraemer, K. Ohno, D.D. Awschalom, A.C. Bleszynski Jayich, Patterned formation of highly coherent nitrogen-vacancy centers using a focused electron irradiation technique, Nano letters 16(4) (2016) 2450-2454.

[15] A.J.P.R.B. Mainwood, Nitrogen and nitrogen-vacancy complexes and their formation in diamond, Phys. Rev. B, 49(12) (1994) 7934.

[16] D. McCloskey, D. Fox, N. O'Hara, V. Usov, D. Scanlan, N. McEvoy, G. Duesberg, G. Cross, H. Zhang, J.F. Donegan, Helium ion microscope generated nitrogen-vacancy centres in type Ib diamond, Applied Physics Letters 104(3) (2014) 031109.

[17] S. Pezzagna, B. Naydenov, F. Jelezko, J. Wrachtrup, J.J.N.J.o.P. Meijer, Creation efficiency of nitrogen-vacancy centres in diamond, New Journal of Physics, 12(6) (2010) 065017.

[18] Y. Liu, G. Chen, M. Song, X. Ci, B. Wu, E. Wu, H. Zeng, Fabrication of nitrogen vacancy color centers by femtosecond pulse laser illumination, Optics express 21(10) (2013) 12843-12848.

[19] S.Z. Chavoshi, S. Goel, P.J.M. Morantz, Design, Current trends and future of sequential micro-machining processes on a single machine tool, Materials & Design, 127 (2017) 37-53.

[20] S. Goel, A topical review on "The current understanding on the diamond machining of silicon carbide", Journal of Physics D: Applied Physics 47(24) (2014) 243001.

[21] Y. Yan, Y. He, Y. Geng, Z. Hu, H. Li, Review on AFM Tip-Based Mechanical Nanomachining: The Influence of the Input Machining Parameters on the Outcomes, Current Nanoscience 12(6) (2016) 666-675.

[22] C.L. Giusca, S.J.P.E. Goel, Improved and simpler estimation of scale linearity contribution to topography measurement, Precision Engineering, 60 (2019) 368-373.

[23] B.A. Myers, A. Das, M. Dartiailh, K. Ohno, D.D. Awschalom, A.B. Jayich, Probing surface noise with depth-calibrated spins in diamond, Physical Review Letters 113(2) (2014) 027602.

[24] R. Fukuda, P. Balasubramanian, I. Higashimata, G. Koike, T. Okada, R. Kagami, T. Teraji, S. Onoda, M. Haruyama, K. Yamada, Lithographically engineered shallow nitrogen-vacancy centers in diamond for external nuclear spin sensing, New Journal of Physics 20(8) (2018) 083029.

[25] J.F. Ziegler, M.D. Ziegler, J.P.J.N.I. Biersack, M.i.P.R.S.B.B.I.w. Materials, Atoms, SRIM–The stopping and range of ions in matter (2010), 268(11-12) (2010) 1818-1823.

[26] M. Hauf, B. Grotz, B. Naydenov, M. Dankerl, S. Pezzagna, J. Meijer, F. Jelezko, J. Wrachtrup, M. Stutzmann, F.J.P.R.B. Reinhard, Chemical control of the charge state of nitrogen-vacancy centers in diamond, Physical Review B, 83(8) (2011) 081304.

[27] G. Irmer, A.J.A.E.M. Dorner-Reisel, Micro-Raman studies on DLC coatings, Adv. Eng. Mater., 7(8) (2005) 694-705.

[28] P.W. May, J.A. Smith, K.N.J.D. Rosser, R. Materials, 785 nm Raman spectroscopy of CVD diamond films, Diamond and related materials, 17(2) (2008) 199-203.

[29] S. Kumar, T.J.T.S.F. Tansley, Structural studies of reactively sputtered carbon nitride thin films, Thin Solid Films, 256(1-2) (1995) 44-47.

[30] G. Sreenivas, S. Ang, W.J.J.o.e.m. Brown, Effects of nitrogen doping on the growth and properties of plasma-enhanced chemical-vapor-deposited diamond-like-carbon films, Journal of electronic materials, 23(6) (1994) 569-575.

[31] J. Orwa, K. Ganesan, J. Newnham, C. Santori, P. Barclay, K. Fu, R. Beausoleil, I. Aharonovich, B. Fairchild, P. Olivero, An upper limit on the lateral vacancy diffusion length in diamond, Diamond and related materials 24 (2012) 6-10.

[32] D. McCloskey, D. Fox, N. O'Hara, V. Usov, D. Scanlan, N. McEvoy, G.S. Duesberg, G.L.W. Cross, H.Z. Zhang, J.F. Donegan, Helium ion microscope generated nitrogen-vacancy centres in type Ib diamond, Appl. Phys. Lett. 104(3) (2014) 031109.

[33] J. Orwa, K. Ganesan, J. Newnham, C. Santori, P. Barclay, K. Fu, R. Beausoleil, I. Aharonovich, B. Fairchild, P.J.D. Olivero, R. Materials, An upper limit on the lateral vacancy diffusion length in diamond, Diamond and Related Materials, 24 (2012) 6-10.

[34] Y.J.P.R.B. Mita, Change of absorption spectra in type-Ib diamond with heavy neutron irradiation, Phys. Rev. B, 53(17) (1996) 11360.

[35] J. Goss, P. Briddon, R. Jones, S.J.D. Sque, R. Materials, Donor and acceptor states in diamond, Diamond and Related Materials, 13(4-8) (2004) 684-690.

[36] Y. Doi, T. Fukui, H. Kato, T. Makino, S. Yamasaki, T. Tashima, H. Morishita, S. Miwa, F. Jelezko, Y.J.P.R.B. Suzuki, Pure negatively charged state of the NV center in n-type diamond, Phys. Rev. B, 93(8) (2016) 081203.

[37] F. Galembeck, T.A. Burgo, Friction and Electrostatics, Chemical Electrostatics, Springer2017, pp. 107-123.

[38] F. Galembeck, T.A. Burgo, L.B. Balestrin, R.F. Gouveia, C.A. Silva, A. Galembeck, Rsc Advances 4(109) (2014) 64280-64298.

[39] B. Brezoczky, H.J.L. Seki, Triboattraction: friction under negative load, Langmuir, 6(6) (1990) 1141-1145.

[40] K. Nakayama, B. Bou-Said, H. Ikeda, Tribo-Electromagnetic Phenomena of Hydrogenated Carbon Films—Tribo-Electrons,-Ions,-Photons, and-Charging, J. Tribol., 119(4) (1997) 764-768.

[41] M. Chen, J.P. Best, I. Shorubalko, J. Michler, R. Spolenak, J.M. Wheeler, Influence of helium ion irradiation on the structure and strength of diamond, Carbon 158 (2020) 337-345.

[42] J. Zhang, X. Wang, B. Shen, F. Sun, International Journal of Refractory Metals and Hard Materials 41 (2013) 285-292.

[43] J.E. Field, The mechanical and strength properties of diamond, Rep. Prog. Phys. 75 (2012) 126505.

[44] J.-P. Tetienne, A. Lombard, D.A. Simpson, C. Ritchie, J. Lu, P. Mulvaney, L.C.L. Hollenberg, Scanning Nanospin Ensemble Microscope for Nanoscale Magnetic and Thermal Imaging, Nano Lett. 16(1) (2016) 326-333.

[45] R.A. Khmelnitsky, V.A. Dravin, A.A. Tal, E.V. Zavedeev, A.A. Khomich, A.V. Khomich, A.A. Alekseev, S.A. Terentiev, Damage accumulation in diamond during ion implantation, J. Mater. Res. 30(09) (2015) 1583-1592.

[46] K. Ohno, F. Joseph Heremans, L.C. Bassett, B.A. Myers, D.M. Toyli, A.C. Bleszynski Jayich, C.J. Palmstrøm, D.D. Awschalom, Engineering shallow spins in diamond with nitrogen delta-doping, Appl. Phys. Lett. 101(8) (2012) 082413.

[47] G. Gubbels, Diamond Turning of Glassy Polymers, PhD Thesis, Technische Universiteit Eindhoven, Eindhoven, 2006. P. 35-39, (2006).

2020-04-27

Distribution of shallow NV centers in diamond revealed by photoluminescence spectroscopy and nanomachin

Jadidi, Majid Fazeli

Elsevier

Jadidi MF, Özer HO, Goel S, et al., (2020) Distribution of shallow NV centers in diamond revealed by photoluminescence spectroscopy and nanomachining. Carbon, Volume 167, October 2020, pp.114-121

https://doi.org/10.1016/j.carbon.2020.04.086